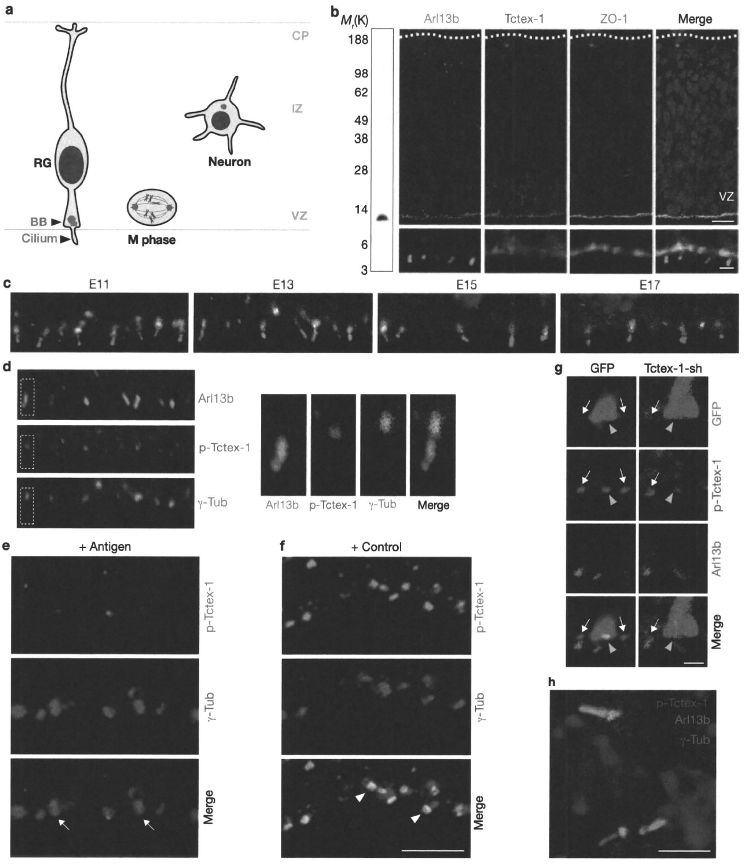

Figure 4 Phospho(T94)Tctex-1 is expressed at the transition zone of radial glia in the developing neocortex. (**a**) Schematic representation of the radially elongated radial glia with their endfeet contacting both the ventricular and pial surfaces. The primary cilium, anchored on a basal body (BB), extends into ventricular spaces. Mitosis (M phase) typically occurs at the ventricular surfaces. Cells leave the cell cycle, migrate away from the ventricular zone (VZ), form multipolar post-mitotic neurons, and pause their migration in the intermediate zone (IZ) before reaching their cortical location. CP; cortical plate. (**b**) Left: anti-Tctex-1 mouse antibody recognized a single band of M_r ~12K on an immunoblot containing embryonic mouse brain lysates. Right: E13 mouse cortical slices were co-labelled for cilium marker Arl13b (ref. 42; green), Tctex-1 (red), and cell–cell junction marker ZO-1 (cy5). Dotted lines represent the ventral borders. Bottom images are enlarged views of the labelling of the ventricle surface. Scale bars, 20 μm (top); 2 μm (bottom). (**c**) Ventricle surfaces of E11–E17 mouse neocortical slices were triple-labelled for Arl13b (green), phospho(T94)Tctex-1 (red) and γ-tubulin (cyan). (**d**) Higher-magnification images (right) of indicated area from an image of an E13 ventricle surface (left; as shown in **c**). Phospho(T94)Tctex-1 (red) was specifically located in the transition zone between the Arl13b-labelled cilia (green) and the γ-tubulin-labelled basal bodies (cyan) of the radial glia. (**e**, **f**) Confocal microscopy images of the ventricular zone from mice brains, double labelled with antibodies against γ-tubulin and phospho(T94) Tctex-1 pre-absorbed with phosphopeptides corresponding to the antigen (**e**) or control peptides (**f**). Arrows in **e** indicate the γ-tubulin-labelled basal bodies and centrosomes, which lacked the phospho(T94)Tctex-1 signal. Arrowheads indicate the phospho(T94)Tctex-1 signals that remained at the ciliary base. Scale bar, 5 μm. (**g**) Co-labelling of phospho(T94) Tctex-1 and Arl13b in mouse cortical slices 24 h after transfection. Note that cells transfected with GFP control plasmid (left, green arrowhead) and neighbouring non-transfected cells (arrows) displayed similar levels of phospho(T94)Tctex-1 at the endfeet. However, cells transfected with Tctex-1-sh (right, green arrowhead) had reduced immunolabelling of phospho(T94)Tctex-1 (arrow indicates neighbouring non-transfected cell). Scale bar, 2 μm. (**h**) Post-mitotic mouse neurons located in the intermediate zone region had no detectable phospho(T94)Tctex-1 (red) between the Arl13-labelled cilia (green) and γ-tubulin-labelled basal bodies (cyan). Scale bar, 5 μm.

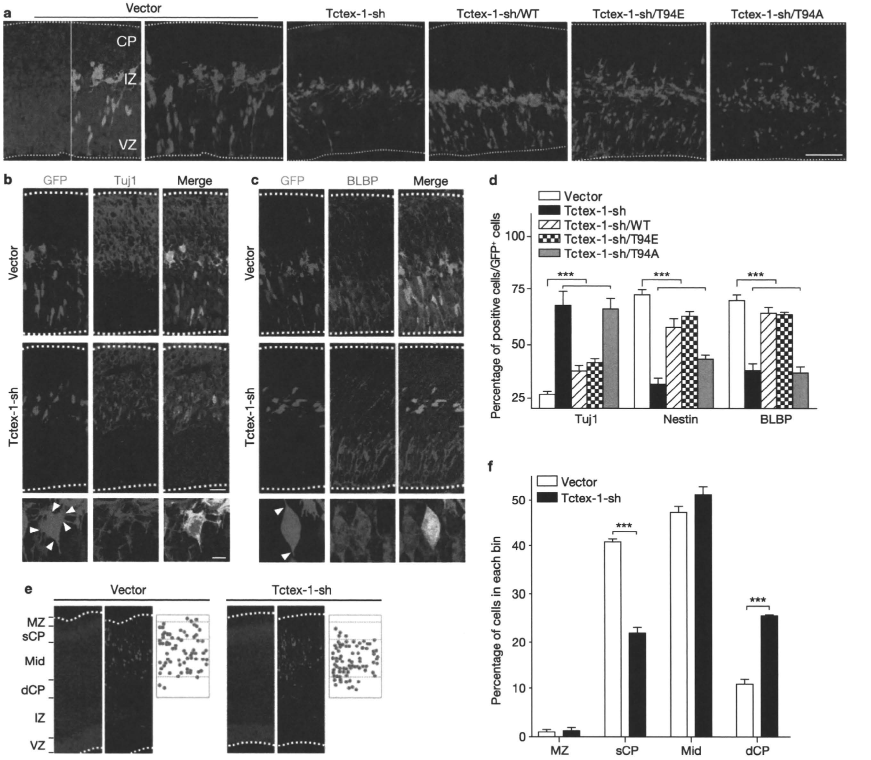

Figure 5 Suppression of Tctex-1 in radial glia induced premature neuronal differentiation. **(a)** Mouse cortical slices harvested 40 h after electroporation with the indicated plasmids. GFP was detected by direct green immunofluoresence microscopy. DAPI; blue. The dashed lines depict the borders of the cortexes. The intermediate zone (IZ) is defined by the presence of tangentially oriented cells. **(b, c)** Representative images showing the labelling of Tuj1 **(b)** and brain lipid-binding protein (BLBP) **(c)** of vector- and Tctex-1-sh-transfected mouse brain slices. Bottom; higher-magnification images of cells transfected with Tctex-1-sh. Arrowheads point to the sites where the cell processes project from the cell bodies. **(d)** Percentage of total transfected GFP$^+$ cells that were Tuj1$^+$, Nestin$^+$ or BLBP$^+$, quantified from an experiment performed as in **c**. Data are means ± s.e.m.; $n = 4$ experiments, except BLBP staining, where $n = 5$ experiments; an average of 600 cells were counted in each experiment; *** $P < 0.001$, one-way ANOVA. **(e)** Representative images depicting the cortical distribution of GFP cells in brains from mice at E18.5 (that is, 5-days post electroporation). Right; plots of GFP$^+$ cell distribution. Top to bottom; the marginal zone (MZ), superficial (sCP), mid-, and deeper cortical plate (dCP) bins were defined as previously described[43] and are as indicated on the images. **(f)** Quantification of the cortical location of transfected cells from experiment performed as in **e** (data are means ± s.e.m.; $n = 3$ experiments; *** $P < 0.001$, *t*-test).

treated quiescent RPE-1 cells with an actin polymerization inhibitor, cytochalasin D (Cyto D), 2 h before serum addition. Cyto D treatment effectively blocked serum-mediated cilium disassembly (Fig. 3c, d). Furthermore, treatment with Cyto D inhibited Tctex-1^{T94E}-peptide-mediated acceleration of ciliary resorption (Fig. 3e). These results imply that phospho(T94)Tctex-1 modulates cilium disassembly through a process involving actin polymerization.

Previous studies have shown that blocking the activation of histone/tubulin deacetylase-6 (HDAC6) mediated by Aurora A kinase (AurA) phosphorylation suppresses cilium resorption in RPE-1 cells[11]. We tested whether AurA- or HDAC6-depleted cells also exhibit impaired S-phase entry. Our results showed that suppression of both AurA and HDAC6 through shRNA or siRNA transfection were able to inhibit both ciliary resorption and BrdU incorporation (Supplementary Fig. S3a-c).

Phospho(T94)Tctex-1 is expressed in the ciliary transition zone of radial glia in the developing neocortex

The developing neocortex is an ideal model system for studying the physiological relevance of phospho(T94)Tctex-1 *in vivo* because the cortical progenitor radial glia also display primary cilia (Fig. 4a), and

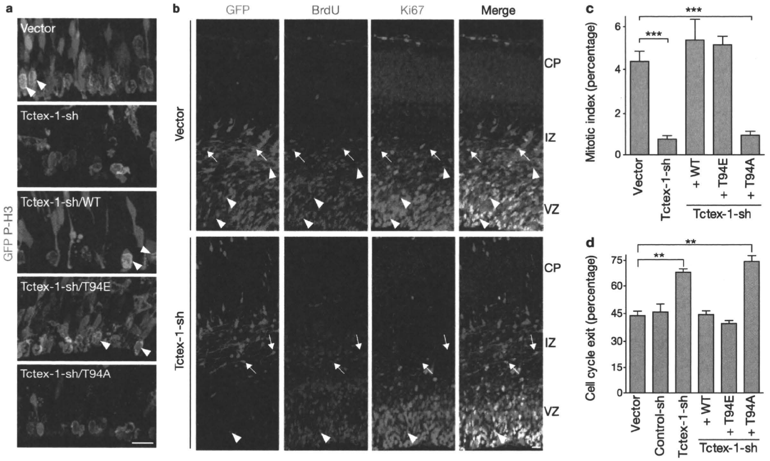

Figure 6 Phosphorylated Tctex-1 is required for cell cycling of radial glia. (**a**) Representative images of the ventricular zone of brains from mice transfected as indicated. Samples were immunolabelled with P-H3. Arrowheads indicate cells that were positive for both GFP and P-H3. (**b**) Representative confocal microscopy images of transfected mouse cortical slices subjected to cell cycle exit analysis. Left, GFP$^+$ cells (green); middle, cells 24 h after BrdU treatment (red) and right, stained with antibodies against Ki67 (cyan). Arrows point to the cells that were positive for GFP and BrdU, but negative for Ki67. Arrowheads point to the cells that were positive for GFP, BrdU and Ki67. (**c**) Fractions of GFP$^+$ and P-H3$^+$ cells out of total GFP$^+$ cells (the mitotic index). Data are means ± s.e.m.; $n = 3$, 6, 3, 5 and 6 experiments for vector, Tctex-sh, Tctex-1-sh/WT, Tctex-1-sh/T94E and Tctex-1-sh/T94A, respectively; *** $P < 0.001$, one-way ANOVA. (**d**) Fractions of GFP$^+$, BrdU$^+$, Ki67$^-$ cells out of total GFP$^+$, BrdU$^+$ cells (or cell cycle exit index). Data are means ± s.e.m.; $n = 3$ experiments; total of 100 cells were scored; ** $P < 0.01$, one-way ANOVA.

the relationship between the cell cycle regulation and the fate control of radial glia has already been established[19,20].

Staining embryonic day (E) 11–E17 mouse embryonic cortices with anti-(pan)Tctex-1 antibody showed that Tctex-1 was specifically concentrated at the apical endfeet of radial glia, from which Arl13b-labelled cilia project into the ventricles (Fig. 4b and Supplementary Fig. S4a). However, phospho(T94)Tctex-1 appeared as prominent punctae lining the ventricular surfaces. Co-localization studies confirmed that phospho(T94) Tctex-1 specifically resides in the transition zone between the γ-tubulin-labelled basal bodies and the primary cilia (Fig. 4c, d). The transition zone-labelling of phospho(T94)Tctex-1 was universal in all radial glia regardless of developmental stage, and despite the fact that there were fewer radial glia in later stages of neurogenesis (that is, E17; Fig. 4c). Preabsorption with the antigen, but not control peptide, effectively removed the phospho(T94)Tctex-1 signals (Fig. 4e, f). Phospho(T94) Tctex-1 labelling was also greatly reduced in radial glia transfected with Tctex-1-sh (Fig. 4g). In marked contrast, no phospho(T94)Tctex-1 signal was detected at the bases of primary cilia in the post-mitotic neurons located at the intermediate zone or cortical plate (Fig. 4h), indicating that phospho(T94)Tctex-1 is present in G_1, but not G_0 cells.

Tctex-1 knockdown triggers premature neuronal differentiation at the expense of the neural progenitor pool

The similar transition zone location of phospho(T94)Tctex-1 in radial glia and cultured ciliated cells prompted us to reason that this molecule may also regulate the cell cycling of Radial glia during corticogenesis. If this were the case, the depletion of Tctex-1 would drive radial glia to exit the cell cycle and differentiate into neurons. Post-mitotic neurons typically migrate away from the ventricular zone where the cell division takes place, halt temporarily at the intermediate zone (Fig. 4a), and are eventually incorporated into laminated cortical plates according to their birthdates[21]. We predicted that excess phospho(T94)Tctex-1 would shorten the G_1 phase, accelerate S-phase entry and expand the progenitor population.

To test our model, we employed *in utero* electroporation (IUE), an efficient gene delivery method for radial glia to perform loss-of-function and gain-of-function analyses. To test the first part of our hypothesis, Tctex-1-sh plasmid was transfected into an E13.5 mouse neocortex. Immunolabelling of cells dissociated from brains harvested as early as 24 h and as late as 5 days after IUE verified the specific knockdown of endogenous Tctex-1 in cells transfected with Tctex-1-sh, but not in cells transfected with control plasmid, (Supplementary Fig. S4b). We subsequently conducted phenotypic characterization of cells transfected with Tctex-1-sh *in situ*. Several lines of evidence suggested that Tctex-1 silencing in radial glia caused their premature neuronal differentiation. First, in cortical slices harvested 40 h after electroporation, cells transfected with control and Tctex-1-sh plasmids displayed strikingly different distribution patterns. Cells transfected with either vector alone (Fig. 5a) or control shRNA plasmid (Supplementary Fig. S4c) were distributed throughout the area between the ventricular zone, subventricular zone and intermediate zone. The large majority of these cells had bipolar shapes and expressed radial glia markers Nestin and brain lipid-binding

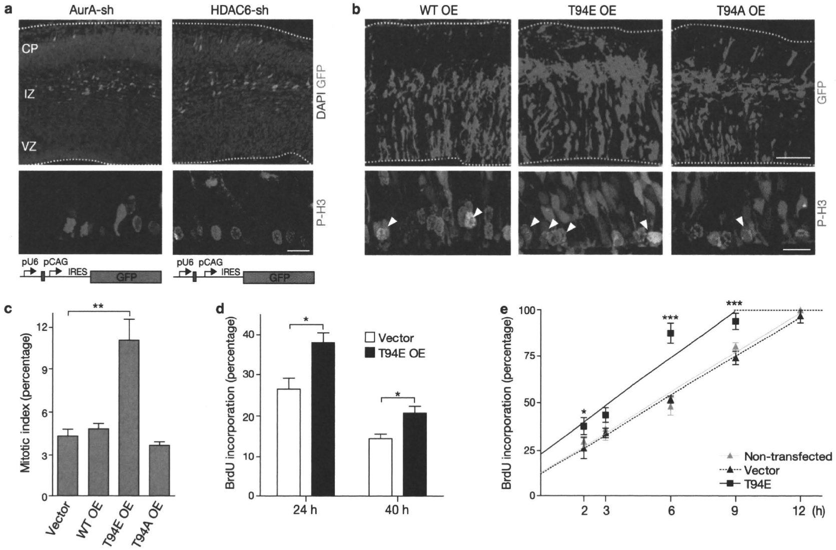

Figure 7 Phenotypic characterization of the developing neocortex of AurA and HDAC6 loss-of-function mutants, and Tctex-1 gain-of-function mutants. **(a)** Mouse cortical slices transfected with AurA-sh or HDAC6-sh plasmid and immunolabelled with P-H3 (red; middle panel). DAPI; blue. Bottom; schematic representation of the respective plasmids. Purple boxes indicate the shRNA-targeting sequences. **(b)** Cortical slices overexpressing the indicated Tctex-1 variants. Arrowheads point to P-H3-labelled, mitotic GFP$^+$ cells at the ventricular zone. Scale bars, 100 μm (top), 20 μm (bottom). **(c)** Mitotic indices of GFP$^+$ cells transfected with plasmids expressing the indicated Tctex-1 variants and GFP. Data are means ± s.e.m.; $n = 3$ experiments; total 1,200 cells were scored; ** $P < 0.01$, one-way ANOVA. **(d)** The fractions of transfected mouse brains with BrdU incorporation (2 h incubation) that were GFP$^+$ cells out of total GFP$^+$ cells, 24 h and 40 h post-electroporation (data are means ± s.e.m.; $n = 4$ experiments; total 700 cells were scored; * $P < 0.05$, t-test). **(e)** Cumulative BrdU labelling curves of non-transfected cells and cells transfected with vector alone or Tctex-1^{T94E}/GFP. Data are means ± s.e.m.; $n = 3$ experiments; * $P < 0.05$, *** $P < 0.001$, one-way ANOVA. OE; overexpression.

protein (Fig. 5c, d), and a much smaller fraction of them displayed post-mitotic neuronal marker Tuj1 (Fig. 5b, d). GFP$^+$ control cells localized to the subventricular zone also displayed intermediate progenitor marker Tbr2 (Supplementary Fig. S4d). In contrast, Tctex-1-silenced GFP$^+$ cells were predominantly concentrated in the intermediate zone (Fig. 5a), bore tangentially radiating multi-polar processes and expressed neuronal marker Tuj1 (Fig. 5b, d). Significantly fewer Tctex-1-sh-targeted cells displayed radial glia markers when compared with the controls (Fig. 5c, d), and almost none of them displayed Tbr2 (Supplementary Fig. S4d).

Second, to corroborate the cell-based phenotypic analysis *in situ*, the fraction of GFP$^+$ cells dissociated from the electroporated brains that also expressed Tuj1 was scored (Supplementary Fig. S4e). These results suggested that a significantly greater number of cells transfected with Tctex-1-sh were neurons. Third, quantitative reverse transcription PCR (RT–PCR) assays using RNAs isolated from flow cytometer-sorted GFP$^+$ cells showed that a significantly higher fraction of Tctex-1-silenced cells expressed Tuj1 in comparison with control cells (data not shown).

A neuron's birthdate is correlated with its laminar fate in the cortical plate as corticogenesis progresses; cells that differentiate at later time points tend to be found in the upper (more superficial) layers of the cortical plate[21]. In agreement with the proposed idea that Tctex-1-sh-targeted cells differentiate and migrate earlier, these cells were found to be located in a relatively deeper cortical layer, compared with the control cells in brains harvested 5 days after IUE (Fig. 5e, f). It was also noted that neurons derived from Tctex-1-sh-targeted cells, similarly to the controls, displayed neuronal markers (for example, HuD and doublecortin) and extended axons (data not shown). These results suggest that Tctex-1 expression is not critical for cell migration. Previous studies have shown that cytoplasmic dynein is important for cortical cell migration[22]. The differences in phenotype seen between the Tctex-1-suppressed and cytoplasmic-dynein-suppressed cells further support the idea that the role of Tctex-1 in corticogenesis is independent of its dynein-related activity.

Tctex-1 suppression drives radial glia exit from the cell cycle

We consistently observed that the total numbers of GFP$^+$ cells in brains transfected with Tctex-1-sh were fewer than those of the control brains (Fig. 5a). This discrepancy in cell number was not due to low transfection efficiency (Supplementary Fig. S5a, b) or apoptotic cell death (Supplementary Fig. S5c). Thus, the most probable explanation is that the Tctex-1-sh-transfected radial glia underwent a premature switch from proliferation to differentiation mode. Early depletion of the fast-proliferating progenitors could result in a detectably lower number of total GFP+ cells because the doubling times for E13–E14 radial glia are rather short (that is, 11.4–15.1 h) [3]. Indeed, compared with control cells, a significantly reduced fraction of Tctex-1-sh-transfected cells exhibited mitotic marker phosphohistone 3 (P-H3; Fig. 6a, c). The low mitotic index also precluded the possibility that Tctex-1-depletion caused mitotic arrest. Furthermore, as expected[23,24], the majority of ventricular zone mitotic cells transfected with vector alone had a vertical cleavage plane (that is, DNA in anaphase/metaphase cells are oriented 60°–90° relative to the axis of ventricle surfaces; Supplementary Fig. S5d). Among the few mitotic cells transfected with Tctex-1-sh, most of them also exhibited vertical cleavage. The difference in the fraction of cells displaying intermediate versus horizontal cleavages between Tctex-1-suppressed and control cells was also negligible.

To test how Tctex-1 knockdown affects cell cycling, we performed a cell cycle exit analysis *in situ*[25]. A single-pulse of BrdU was given to mice 24 h after IUE, and the brain slices harvested 24 h afterwards were immunolabelled for BrdU and Ki67. The fraction of GFP+ BrdU+ cells that were Ki67− (that is, cell-cycle-exit index) was found to be greater in cells transfected with Tctex-1-sh than in control cells (Fig. 6b, d).

All phenotypes elicited by Tctex-1 silencing—the distribution and number of transfected cells (Fig. 5a), the neuron-to-progenitor ratio (Fig. 5d), the mitotic indices (Fig. 6 c) and the cell-cycle-exit indices (Fig. 6d)—were successfully restored by both wild-type and Tctex-1^{T94E}, but not by Tctex-1^{T94A}. Taken together, these results suggest that phospho(T94)Tctex-1 is the active form of Tctex-1 in radial glia.

Phospho-mimic Tctex-1 accelerates S-phase entry and increases the proliferating progenitor population

If impaired ciliary disassembly caused by Tctex-1 silencing underlies the S-entry block of radial glia, the perturbation of a known inhibitor of cilium resorption should mimic the phenotypes exerted by Tctex-1-sh. Indeed, the majority of cells transfected with plasmids encoding *AurA* shRNA (AurA-sh) or *HDAC6* shRNA (HDAC6-sh) developed into intermediate-zone-residing neurons 40 h after electroporation (Fig. 7a), and displayed significantly lower mitotic indices (mitotic indices of AurA-sh and HDAC-6-sh transfected cells were 1% and 0.5%, respectively, versus 4.4% of control cells).

To carry out gain-of-function analysis, bicistronic vectors expressing both Tctex-1 (or its variants) and GFP were employed to perform IUE. We first showed that overexpression of Tctex-1^{T94E}, but not wild-type or Tctex-1^{T94A}, almost doubled the mitotic index in transfected neocortices (Fig. 7b, c). Furthermore, cell-cycle entry analysis, in which a single pulse of BrdU was given to the mice 2 h before harvest was carried out. The fraction of GFP+ cells that were also BrdU+ was significantly higher in cells transfected with Tctex-1^{T94E} than in those transfected with wild-type Tctex-1 or Tctex-1^{T94A} (Fig. 7d), suggesting that S-phase entry is accelerated in Tctex-1^{T94E}-overexpressing cells. Finally, we employed a cumulative BrdU labelling experiment to determine the cell cycle length of the radial glial cells[3]. The length of the G_2/M phase of Tctex-1^{T94E}-, GFP- and non-transfected progenitors was the same (2 h). However, the G_1 length of Tctex-1^{T94E}-transfected progenitors (6.8 h) was significantly shorter than that of untransfected or GFP-transfected progenitors (10 h; Fig. 7e). These results suggest that forced expression of phospho-mimic Tctex-1 expands the proliferating progenitor pool by shortening the G_1 phase and accelerating S-phase re-entry.

DISCUSSION

Human genetic studies have suggested a causal relationship between several ciliary/centrosomal proteins and the cellular overproliferation phenotype seen in cilium-related disorders, such as cystic kidney disease and certain brain development diseases[26]. However, the relationships between cilia, centrosomes and cell division are not well understood. Complete ciliary resorption before mitosis is thought to be necessary for the release of centrioles from basal bodies to form mitotic poles[18]. Several ciliated proteins have indeed been linked to the G_2/M transition and/or to cytokinesis[27,28]. The significance of ciliary shortening at late-G_1 phase and its relevance to the subsequent S-phase entry, however, is unknown. Here we present evidence that phospho(T94)Tctex-1 is required for cilium resorption, and hence S-phase entry.

Our data supports a model in which cilia provide a brake in the cell cycle to retain cells in G_0/G_1. Extracellular cues that activate the signalling pathways involved may determine the time required for this cellular event to take place and the duration of G_0/G_1. Cilia-mediated quiescence control may be absent in some non-ciliated cancerous cells[29]. These cells are thus likely to be insensitive to the environmental cues that time normal cells for division.

An understanding of the molecular switch between self-renewal and neuronal differentiation in cortical progenitors is critical in elucidating mechanisms that control brain size[30–32]. We speculate that radial glia receive ventricular cues via the cilium, allowing for subsequent recruitment of phospho(T94)Tctex-1 to guide timely ciliary resorption and proliferation. Blocking the activation of phospho(T94)Tctex-1 induces neuronal differentiation at the expense of proliferating progenitors, mimicking the developmental programme of late progenitors. Interestingly, several protein mutations found in human diseases associated with small brain size are localized to the centrosomes[33]. Although both previous[4,5,19,20] and our studies suggest G_1 length controls the cell fate determination of radial glia during corticogenesis, direct visualization and comparison of life cycle of radial glia with varying G_1 lengths remains to be shown.

The primary cilium is vital for the proper development of multiple brain regions. Sonic hedgehog signalling pathway transduced through cilia delivers a proliferative signal, which is required for the establishment and maintenance of neural progenitors of the cerebellum and hippocampus[34–3637]. Thus, it seems that while the cilia are required to sense 'proliferation' signals, they are resorbed in a timely manner to permit the cells to re-enter the cell cycle. These two seemingly opposing roles of cilia could represent two temporally related events, working in conjunction to regulate cell division.

A link between the spindle orientation and the fate determination of mouse radial glia has been previously proposed[38], but remains controversial[23,24]. We did not observe any significant change in spindle orientation in Tctex-1 suppressed cells, suggesting that altering the cleavage plane was not a major contributor to the neural fate adoption of these cells. This finding differed from a previous report[39] where it was suggested that suppression of Tctex-1 expression has an impact on the spindle orientation of radial glia. Differences were noted between these two studies. First, different *Tctex-1* shRNA plasmids were used; we were able to rule out any off-target effect by performing *in vivo* rescue experiments. Second, we considered cells with cleavage plane at an angle greater than or equal to 30° oblique to the vertical plane to be anomalous[23,24,38]; the previous study considered 15° to be the reference point[39].

A recent report suggested that actin dynamics is involved in ciliogenesis[40]. Our data show that phospho(T94)Tctex-1-regulated ciliary resorption also occurs through a process involving actin cytoskeleton rearrangement. We envision that at the base of the cilium, Tctex-1 is dissociated from the dynein complex, through phosphorylation at Thr 94. Phosphorylated Tctex-1 activates local F-actin polymerization, which may trigger a cascade of cellular events that coordinately resorb the cilia and modify the basal bodies. The latter may transmit signals to programme the cells for S-phase entry, a mechanism that agrees with the finding that the centrosome/basal body is a central hub for almost all cell cycle-regulating proteins[41].

METHODS

Methods and any associated references are available in the online version of the paper at http://www.nature.com/naturecellbiology/

Note: Supplementary Information is available on the Nature Cell Biology website

ACKNOWLEDGEMENTS

We are indebted to the following grant support: Tri-Institutional Starr Foundation, NYSTEM, NIH (EY11307, EY016805), RPB (to C-H.S.), Tohoku University (to M.S.), New Energy and Industrial Technology Development Organization, and Grant-in-Aid for Scientific Research from the Ministry of Education, Science, Sports, and Culture of Japan (to K.T.). We thank G. Pazour, K. Anderson, R. Hevner, Y. Shi, N. Heintz, C. Cepko, A. Liu and S. Doxsey for reagents, and S. Anderson, M. E. Ross, D. Cobrinik and B. Tsou for discussion.

AUTHOR CONTRIBUTIONS

A.L., J-Z.C. and C-H.S designed the overall study. A.L. and C.D. performed IUE experiments and phenotype characterization. J-Z. C. generated all constructs. A. L., Y-Y.T. and M.S. performed cell culture studies. K.T. generated the anti-phospho(T94)Tctex-1 antibody. K.T. and T.K. generated 9R peptides. A.L., J-Z.C. and C-H.S. wrote the paper.

COMPETING FINANCIAL INTEREST STATEMENT

The authors declare that they have no competing financial interests.

Published online at http://www.nature.com/naturecellbiology
Reprints and permissions information is available online at http://npg.nature.com/reprintsandpermissions/

1. Pan, J. & Snell, W. The primary cilium: keeper of the key to cell division. *Cell* **129,** 1255–1257 (2007).
2. Alvarez-Buylla, A., Garcia-Verdugo, J. M. & Tramontin, A. D. A unified hypothesis on the lineage of neural stem cells. *Nat. Rev. Neurosci.* **2,** 287–293 (2001).
3. Takahashi, T., Nowakowski, R. S. & Caviness, V. S., Jr. The cell cycle of the pseudostratified ventricular epithelium of the embryonic murine cerebral wall. *J. Neurosci.* **15,** 6046–6057 (1995).
4. Lange, C., Huttner, W. B. & Calegari, F. Cdk4/cyclinD1 overexpression in neural stem cells shortens G1, delays neurogenesis, and promotes the generation and expansion of basal progenitors. *Cell Stem Cell* **5,** 320–331 (2009).
5. Pilaz, L. J. *et al.* Forced G1-phase reduction alters mode of division, neuron number, and laminar phenotype in the cerebral cortex. *Proc. Natl Acad. Sci. USA* **106,** 21924–21929 (2009).
6. Calegari, F. & Huttner, W. B. An inhibition of cyclin-dependent kinases that lengthens, but does not arrest, neuroepithelial cell cycle induces premature neurogenesis. *J. Cell Sci.* **116,** 4947–4955 (2003).
7. Pfister, K. K. *et al.* Cytoplasmic dynein nomenclature. *J. Cell Biol.* **171,** 411–413 (2005).
8. King, S. M. *et al.* The mouse *t*-complex-encoded protein Tctex-1 is a light chain of brain cytoplasmic dynein. *J. Biol. Chem.* **271,** 32281–32287 (1996).
9. Chuang, J. Z. *et al.* The dynein light chain Tctex-1 has a dynein-independent role in actin remodeling during neurite outgrowth. *Dev. Cell* **9,** 75–86 (2005).
10. Dedesma, C., Chuang, J. Z., Alfinito, P. D. & Sung, C. H. Dynein light chain Tctex-1 identifies neural progenitors in adult brain. *J. Comp. Neurol.* **496,** 773–786 (2006).
11. Pugacheva, E. N., Jablonski, S. A., Hartman, T. R., Henske, E. P. & Golemis, E. A. HEF1-dependent Aurora A activation induces disassembly of the primary cilium. *Cell* **129,** 1351–1363 (2007).
12. Mittnacht, S. Control of pRB phosphorylation. *Curr. Opin. Genet. Dev.* **8,** 21–27 (1998).
13. Follit, J. A., Tuft, R. A., Fogarty, K. E. & Pazour, G. J. The intraflagellar transport protein IFT20 is associated with the Golgi complex and is required for cilia assembly. *Mol. Biol. Cell* **17,** 3781–3792 (2006).
14. Jia, J. *et al.* Suppressor of Fused inhibits mammalian Hedgehog signaling in the absence of cilia. *Dev. Biol.* **330,** 452–460 (2009).
15. Murcia, N. S. *et al.* The Oak Ridge Polycystic Kidney (orpk) disease gene is required for left-right axis determination. *Development* **127,** 2347–2355 (2000).
16. Tucker, R. W., Pardee, A. B. & Fujiwara, K. Centriole ciliation is related to quiescence and DNA synthesis in 3T3 cells. *Cell* **17,** 527–535 (1979).
17. Schneider, L. *et al.* PDGFRαα signaling is regulated through the primary cilium in fibroblasts. *Curr. Biol.* **15,** 1861–1866 (2005).
18. Matsushita, M. *et al.* A high-efficiency protein transduction system demonstrating the role of PKA in long-lasting long-term potentiation. *J. Neurosci.* **21,** 6000–6007 (2001).
19. Dehay, C. & Kennedy, H. Cell-cycle control and cortical development. *Nat. Rev. Neurosci.* **8,** 438–450 (2007).
20. Gotz, M. & Huttner, W. B. The cell biology of neurogenesis. *Nat. Rev. Mol. Cell Biol.* **6,** 777–788 (2005).
21. Kriegstein, A. R. & Noctor, S. C. Patterns of neuronal migration in the embryonic cortex. *Trends Neurosci.* **27,** 392–399 (2004).
22. Shu, T. *et al.* Ndel1 operates in a common pathway with LIS1 and cytoplasmic dynein to regulate cortical neuronal positioning. *Neuron* **44,** 263–277 (2004).
23. Konno, D. *et al.* Neuroepithelial progenitors undergo LGN-dependent planar divisions to maintain self-renewability during mammalian neurogenesis. *Nat. Cell Biol.* **10,** 93–101 (2008).
24. Morin, X., Jaouen, F. & Durbec, P. Control of planar divisions by the G-protein regulator LGN maintains progenitors in the chick neuroepithelium. *Nat. Neurosci.* **10,** 1440–1448 (2007).
25. Chenn, A. & Walsh, C. A. Regulation of cerebral cortical size by control of cell cycle exit in neural precursors. *Science* **297,** 365–369 (2002).
26. Davenport, J. R. & Yoder, B. K. An incredible decade for the primary cilium: a look at a once-forgotten organelle. *Am. J. Physiol. Renal Physiol.* **289,** F1159–1169 (2005).
27. Mahjoub, M. R., Qasim Rasi, M. & Quarmby, L. M. A NIMA-related kinase, Fa2p, localizes to a novel site in the proximal cilia of *Chlamydomonas* and mouse kidney cells. *Mol. Biol. Cell* **15,** 5172–5186 (2004).
28. Qin, H., Wang, Z., Diener, D. & Rosenbaum, J. Intraflagellar transport protein 27 is a small G protein involved in cell-cycle control. *Curr. Biol.* **17,** 193–202 (2007).
29. Seeley, E. S., Carriere, C., Goetze, T., Longnecker, D. S. & Korc, M. Pancreatic cancer and precursor pancreatic intraepithelial neoplasia lesions are devoid of primary cilia. *Cancer Res.* **69,** 422–430 (2009).
30. Fish, J. L., Kosodo, Y., Enard, W., Paabo, S. & Huttner, W. B. Aspm specifically maintains symmetric proliferative divisions of neuroepithelial cells. *Proc. Natl Acad. Sci. USA* **103,** 10438–10443 (2006).
31. Higginbotham, H. R. & Gleeson, J. G. The centrosome in neuronal development. *Trends Neurosci.* **30,** 276–283 (2007).
32. Zhong, X., Pfeifer, G. P. & Xu, X. Microcephalin encodes a centrosomal protein. *Cell Cycle* **5,** 457–458 (2006).
33. Bond, J. & Woods, C. G. Cytoskeletal genes regulating brain size. *Curr. Opin. Cell Biol.* **18,** 95–101 (2006).
34. Chizhikov, V. V. *et al.* Cilia proteins control cerebellar morphogenesis by promoting expansion of the granule progenitor pool. *J. Neurosci.* **27,** 9780–9789 (2007).
35. Spassky, N. *et al.* Primary cilia are required for cerebellar development and Shh-dependent expansion of progenitor pool. *Dev. Biol.* **317,** 246–259 (2008).
36. Han, Y. G. *et al.* Hedgehog signaling and primary cilia are required for the formation of adult neural stem cells. *Nat. Neurosci.* **11,** 277–284 (2008).
37. Lai, K., Kaspar, B. K., Gage, F. H. & Schaffer, D. V. Sonic hedgehog regulates adult neural progenitor proliferation *in vitro* and *in vivo*. *Nat. Neurosci.* **6,** 21–27 (2003).
38. Chenn, A. & McConnell, S. K. Cleavage orientation and the asymmetric inheritance of Notch1 immunoreactivity in mammalian neurogenesis. *Cell* **82,** 631–641 (1995).
39. Gauthier-Fisher, A. *et al.* Lfc and Tctex-1 regulate the genesis of neurons from cortical precursor cells. *Nat. Neurosci.* **12,** 735–744 (2009).
40. Kim, J. *et al.* Functional genomic screen for modulators of ciliogenesis and cilium length. *Nature* **464,** 1048–1051 (2010).
41. Doxsey, S., Zimmerman, W. & Mikule, K. Centrosome control of the cell cycle. *Trends Cell Biol.* **15,** 303–311 (2005).
42. Caspary, T., Larkins, C. E. & Anderson, K. V. The graded response to Sonic Hedgehog depends on cilia architecture. *Dev. Cell* **12,** 767–778 (2007).
43. Takeuchi, A. & O'Leary, D. D. Radial migration of superficial layer cortical neurons controlled by novel Ig cell adhesion molecule MDGA1. *J. Neurosci.* **26,** 4460–4464 (2006).

METHODS

Cell cultures, transfection and cilium assembly/disassembly assay. IFT20KD-RPE-1 was a gift from G. Pazour[13] (University of Massachussets Medical School; USA). Immortalized wild-type MEF and *Ift88* mutant MEF cells were gifts from A. Liu[14] (Pennsylvania State University, USA). MEF, RPE-1 and 3T3 cells were transfected using nucleofection (Amaxa). HeLa cells were transfected using Lipofectamine 2000 (Invitrogen). COS-7 and HEK cells were transfected using the polyethylenimine method[44]. Protein expression levels were estimated by immunoblotting and quantified by Odyssey Infrared scanner (LI-COR). For most immunolabelling, cultured cells were fixed in 4% paraformaldehyde for 10 min and then submerged in cold methanol for 5 min before the blocking and antibody incubation using standard procedures.

A cilium assembly/disassembly assay was performed as previously described[11]. Specifically, cells were starved in serum-free medium for 48 h to induce cilium formation. Serum was then added back to the medium to stimulate cilium resorption and cell cycle re-entry. Cells were harvested at various time points for immunolabelling assays. All plasmids used for overexpression experiments in cultures were under the CMV promoter. Cells receiving more than one plasmid were routinely immunolabelled to confirm high (> 90%) double or triple transfection efficiency.

Purified recombinant proteins (for example, GFP-9R, Tctex-$1^{T94E\text{-}9R}$ and Tctex-$1^{T94A\text{-}9R}$; 1 μM) were added into cilium-preformed cells in the absence of serum for 30 min[18]. Cells were then gently rinsed and transferred to peptide-free, serum-free medium for different time periods before fixation. In some experiments, Cyto D (0.5 μM, Sigma) was included in the medium 1 h before the peptide addition and thereafter.

BrdU incorporation index. For the experiments carried out in synchronized cells, 12-hr post-transfected cells were induced to growth arrest by 48 h serum starvation. Cells were then cultured in regular medium for 12 hr, pulse labelled with 1 hr BrdU (10 μM), and followed by a 12 hr chase. These cells were subsequently treated with acid followed by BrdU labelling. The fractions of GFP$^+$ transfected cells with BrdU incorporated were counted, and the BrdU incorporation indices were shown by considering the control as 100%. For the experiments carried out in unsynchronized cells, cells 48 hr post-transfection wee treated with BrdU for 12 hr, followed by GFP and BrdU labelling. For the protein transduction experiments, BrdU was added into serum-free medium for 12hr immediately after the 30-min incubation of peptides.

IUE, immunohistochemistry of mouse brain slices, and quantitative analyses. IUE procedures were performed on E13.5 CD1 mouse brains using plasmids driven by either CAG or U6 promoter, as described[45]. At specific time points, electroporated brains were harvested, fixed with 4% paraformaldehyde overnight at 4°C, embedded in low melting agarose, and sectioned by vibratome. Sectioned brain slices were subsequently subjected to immunostaining. For the ventricle surfaces of E11–E17 neocortical slices, triple-labelled for Arl13b, Tctex-1 phosphorylated at Thr 94 and γ-tubulin, cortical slices were first incubated with antibody against Tctex-1 phosphorylated at Thr 94, followed by excess biotinylated goat-anti-rabbit antibody. The sections were then PFA fixed, incubated with anti-Arl13b and γ-tubulin antibodies, followed by detection by using Alexa488-conjugated anti-rabbit, Cy5-conjugated anti-mouse antibody, and Alexa568-conjugated streptavidin. All immunolabelled sections were analysed by Leica TCS SP2 spectral confocal system (Nussloch, Germany), as previously described[10]. In some experiments, electroporated brains were dissociated with papain (Worthington) and dispersed on poly-L-lysine coated coverslips. After a 2-h 37°C incubation, cells were fixed with 4% paraformaldehyde followed by immunostaining. All animal manipulations were performed in accordance with the guidelines for animal experiments at Weill Medical Cornell IACUC.

Mitotic index, cell-cycle exit and cell-cycling analyses in brain slices. The mitotic index of treated brain slices was determined as the ratios of GFP$^+$ and P-H3$^+$ cells to the total GFP$^+$ transfected cells in the ventricular zone/subventricular zone. Cell cycle analysis was performed as described[46]. Briefly, pregnant mice were injected with BrdU (50 mg per kg body weight) 24 h after IUE, and fetal brains were harvested 24 h after BrdU treatment. Brain slices were then immunolabelled for GFP, BrdU and Ki67. The cell-cycle-exit index of GFP-transfected cells was determined as a ratio of the GFP-labelled cells that exited the cell cycle (GFP$^+$, BrdU$^+$ and Ki67$^-$) to total GFP-labelled cells with BrdU incorporation (GFP$^+$ and BrdU$^+$). For S-phase entry analysis, IUE-treated animals were treated with BrdU (50 mg per kg body weight) for 2 h before harvest. In all cases, similar areas in the transfected neocortices were selected for analysis. Calculation of cell cycle phases was carried out using cumulative BrdU incorporation, as described[3]. Briefly, BrdU injection started at E14.5 (24 h post-electroporation) and continued at 3-h intervals. Mice were sacrificed 2, 3, 6, 9 or 12 h after the first BrdU injection. 100% BrdU incorporation refers to when all ventricular zone cells are labelled with BrdU. The length of G_2/M was taken to be the time required to label all mitotic cells, based on chromatin condensation. The length of G_1 was estimated as described[3].

Production and specificity verification of phospho-specific antibodies for Tctex-1. Rabbits were injected with a peptide (TDGSC(pT)VRWEN) corresponding to amino-acid positions 89–99 of human Tctex-1 with chemical phosphorylation on the Thr 94 residue. The resulting serum was affinity purified with a phospho-peptide column. The affinity-purified antibody specifically detected the phosphorylated peptide but not the unphosphorylated peptide in an ELISA (enzyme-linked immunosorbent assay).

Reagents. Two human *Tctex-1*-siRNA oligonucleotides (targeting sequence: 5′-GAGGCTAUAGAAAGCGCAATT-3′ and 5′-TACATCGTGACCTGTGTAATT-3′) and a mouse Tctex-1-siRNA (targeting sequence: 5′-GTCAACCAGTGGACCACT-3′) were synthesized by Thermo Fisher (Waltham). Both control-siRNA and AurA-siRNA oligonucleotide were purchased from Santa Cruz Biotech (Santa Cruz). To generate short-hairpin encoding plasmid, the annealed targeting-oligonucleotides were first inserted into pU6-promoter-driven vector (gift of Y. Shi, Harvard University, USA), as suggested[47]. The entire shRNA expression cassette was then transferred into pCAG-IRES-GFP vector (gift from C. Cepko, Harvard University, USA); the resulting construct thus also encoded GFP under the CAG promoter. The targeting sequences for mouse and human *Tctex-1* shRNA were 5′-GGGTTACACTCCGCAAGTTCC-3′ and 5′-GGGACAGCTCTACTGACGGGA-3′, respectively. The targeting sequence for (mouse and human) *HDAC6* shRNA was 5′-GGGTTATGCCCACCTCACCCAC-3′. Three control shRNA plasmids were used; one was purchased from Applied Biosystem (Austin, TX) and two were synthesized (the targeting sequences were 5′-GGGATCGTAGGTTCTCGAAA-3′ and 5′-GGGCTATACCAAGAGACATGC-3′). For ectopic expression *in vivo*, cDNA fragments encoding Tctex-1 (e.g.,wild-type, Tctex-1^{T94E} or Tctex-1^{T94A}; ref. 9) were cloned into either pCAG-IRES-GFP or Tctex-1-sh/GFP plasmid. pRK5 vector encoding wild-type, Tctex-1^{T94E}, and Tctex-1^{T94E}, described in ref.9, were used to perform the *in vitro* expression. GFP-9R and Tctex-1-9R were generated in pET21a vector (Novagen), and recombinant proteins were expressed in BL21 (DE3) cells and purified by Ni-NTA agarose column (Invitrogen)[18].

The primary antibodies used were: acetylated α-tubulin mouse immmunoglobulin G2b (IgG_{2b}; 1:400, Sigma), Arl13b rabbit antibody (1:500, gift from K. Anderson[42], Memorial-Sloan Kettering Cancer Center, USA), α-tubulin mouse antibody (1:1,000, GE Health), brain lipid-binding protein rabbit antibody (1:2,500, gift from N. Heintz[48], Rockefeller University, USA), BrdU rat antibody (1:200, Harlan), active caspase 3 rabbit antibody (1:200, Abcam), dynein intermediate chain mouse antibody (1:10,000, Millipore), Flag mouse and rabbit antibodies (1:500, Sigma), GFP rabbit antibody (1:1,000, Invitrogen), GFP chicken antibody (1:2,000, Abcam), GFP mouse antibody (1: 1,000, Millipore), γ-tubulin mouse antibody (clone GTU-88, immunoglobulin G1, IgG_1; 1: 2,000, Sigma), Ki67 rabbit antibody (1:500, Novocastra), Nestin mouse antibody (clone 401, 1: 200, Developmental Studies Hybridoma Bank), P-H3 rabbit antibody (1:200, Millipore), Tbr2 rabbit antibody (1:1,000, gift from R. Hevner[49], University of Washington School of Medicine, USA), protein A-purified Tctex-1 mouse antibody (1:1,000, this paper), affinity-purified Tctex-1 rabbit antibody[50] (1:100), Tuj1 mouse antibody (1:500, Covance), ZO-1 mouse antibody (1:500, Invitrogen), phospho-Rb (Ser795), phospho-Rb(Ser807/811), and phospho-cdc2 (Tyr15) rabbit antibodies (1:1,000, Cell Signalling Technology). Alexa-conjugated streptavidin or secondary antibodies (anti-mouse, anti-rabbit, anti-rat, anti-IgG_{2b}; 1:400) were purchased from Invitrogen; biotinylated anti-IgG_1 and Cy5-conjugated streptavidin were purchased from Jackson Lab (used at 1:200; West Grove). In this study, negative controls involved omission of the primary antibody and use of antibody that had been pre-absorbed with antigen. Co-labelling of acetylated α-tubulin (mouse IgG_{2b}) and γ-tubulin (mouse IgG_1) in this study involved using isotype-specific mouse immunoglobulins.

DOI: 10.1038/ncb2218

Microscopic and statistical analyses. All the quantification studies were carried out in transfected cells localized within the dorsolateral neocortex to avoid possible variation within particular brain regions. At least three independent brains were analysed for each DNA construct. Analysis of the immunostained sections was carried out on a Leica TCS SP2 spectral confocal system. To improve observer objectivity, image capture and analysis were done at separate times in a double-blind fashion. To score images, the GFP channel was first judged independently, followed by judgments of the other markers. For Ki67 and BrdU-nuclear labelling, small puncta or signals that were not compliant with the DAPI (4,6-diamidino-2-phenylindole) nuclear labelling were ignored.

Statistical analysis was performed with GraphPad software (GraphPad Prism v4.0, GraphPad Software). Data are presented as the mean ± s.e.m. from at least three representative independent experiments. *t*-test was designed for the comparison of two groups. One-way analysis of variance (ANOVA) was applied for the comparisons in which only one independent variable was being analysed. The Dunnet test (as a *post hoc* test) was used to compare data samples versus control. Statistical significance was defined as $P < 0.05$, 0.01 or 0.001.

44. Thomas, M. *et al.* Full deacylation of polyethylenimine dramatically boosts its gene delivery efficiency and specificity to mouse lung. *Proc. Natl Acad. Sci. USA* **102,** 5679–5684 (2005).
45. Tabata, H. & Nakajima, K. Efficient *in utero* gene transfer system to the developing mouse brain using electroporation: visualization of neuronal migration in the developing cortex. *Neuroscience* **103,** 865–872 (2001).
46. Sanada, K. & Tsai, L. H. G protein βγ subunits and AGS3 control spindle orientation and asymmetric cell fate of cerebral cortical progenitors. *Cell* **122,** 119–131 (2005).
47. Xia, X. G. *et al.* An enhanced U6 promoter for synthesis of short hairpin RNA. *Nucleic Acids Res.* **31,** e100 (2003).
48. Feng, L., Hatten, M. E. & Heintz, N. Brain lipid-binding protein (BLBP): a novel signaling system in the developing mammalian CNS. *Neuron* **12,** 895–908 (1994).
49. Hevner, R. F. *et al.* Tbr1 regulates differentiation of the preplate and layer 6. *Neuron* **29,** 353–366 (2001).
50. Tai, A. W., Chuang, J.-Z. & Sung, C.-H. Localization of Tctex-1, a cytoplasmic dynein light chain, to the Golgi apparatus and evidence for dynein complex heterogeneity. *J. Biol. Chem.* **273,** 19639–19649 (1998).

nature
cell biology

DOI: 10.1038/ncb2218

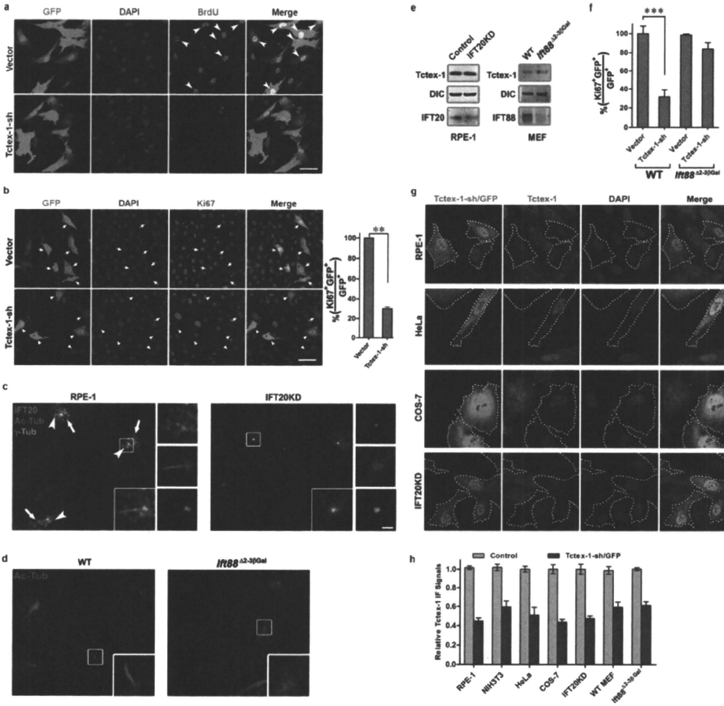

Figure S1 (**a**) BrdU labeling of RPE-1 cells transfected with vector or Tctex-1-sh. Arrowheads point to cells double positive for GFP and BrdU. (**b**) (Left) Ki67 labeling of RPE-1 cells transfected with vector or Tctex-1-sh. Arrows point to cells double positive for Ki67 and GFP; arrowheads point to the cells positive for GFP and negative for Ki67. (Right) Quantification of the percentage of Ki67$^+$GFP$^+$ cells out of total GFP$^+$ cells (mean±s.e.m.; n=3 experiments; **p<0.01, *t*-test). (**c**) Immunolabeling of serum-starved RPE-1 and IFT20KD-RPE-1 cells for IFT20 (green), acetylated a-tubulin (red), and g-tubulin (cyan). These results showed that, consistent with the previous report, the endogenous IFT20 immunoreactivity was enriched at the Golgi apparatus in the parental RPE-1 cells (arrows), but diminished in the IFT20KD-RPE-1 cells. Enlarged boxed areas showed that the primary cilia (arrowheads) were readily detectable in RPE-1 cells, but not in IFT20KD-RPE-1 cells. Cytoplasmic acetylated a-tubulin labeling remains, however, detectable in the latter. (**d**) Acetylated a-tubulin immunolabeling verified the presenceand absence of primary cilia in WT and *Ift88* mutant MEF cells, respectively. (**e**) Immunoblots showed specific reduction of endogenous IFT20 in IFT20-KD RPE cells and specific depletion of IFT88 in *Ift88* mutant MEF cells. The levels of Tctex-1 and DIC were not affected in these cells. (**f**) Fractions of Ki67-labeled cells in GFP$^+$ transfected cells are shown (mean ± s.e.m.; n=3 experiments; ***p<0.001, *t*-test). (**g**) Representative images show endogenous Tctex-1 immunofluorescence (red) were specifically reduced in cells transfected with Tctex-1-sh/GFP plasmids. Dotted lines depict the cell borders. (**h**). Quantification of Tctex-1 immunofluorescence between untransfected (control) and Tctex-1-sh transfected cells. An average of 20 cells were scored for each group. Bars= 50 mm (a, b), 2 mm (c), 10mm (g).

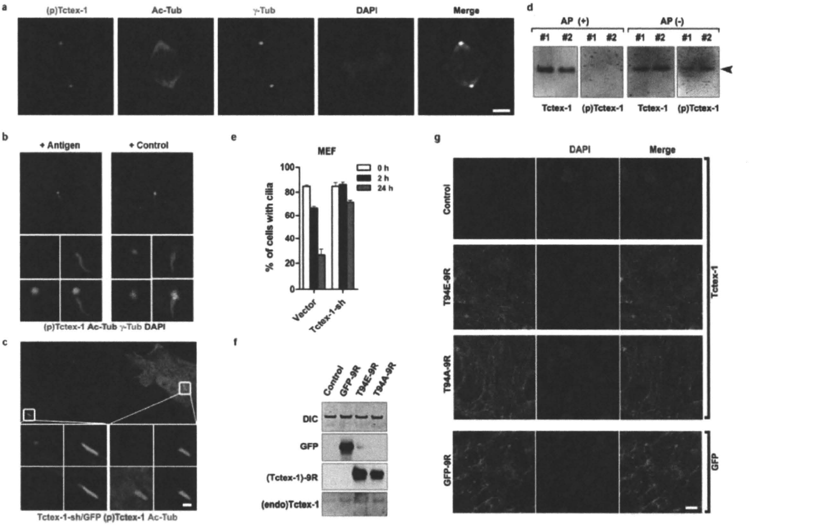

Figure S2 (a) 24-hr post-serum RPE-1 cells immunolabeled for phosph(T94)Tctex-1 (green), acetylate-a-tubulin (red), and g-tubulin (cyan). Bar=5 mm. **(b)** 2-hr post-serum RPE-1 RPE-1 cells were labeled with Ab recognizing phospho(T94)Tctex-1 (green) that was preabsorbed with phosphopeptides corresponding to the antigen (left) or control non-phosphopeptides (right). Acetylated a-tubulin (red) and g-tubulin (cyan) were also co-labeled. **(c)** Immunolabeling of 2-hr postserum RPE-1 cells showed that phospho(T94)Tctex-1 was present at the ciliary bases of untransfected cells, but was absent from the GFP+, Tctex-1-sh plasmid transfected cells. Bar= 2 mm. **(d)** Protein blots containing two independent duplicates (#1 and #2) of RPE-1 cell lysates harvested at 24-hr post-serum time points. These blots were either treated (+) or not treated (-) by alkaline phosphatase (AP), and followed by Tctex-1 or phospho(T94)Tctex-1 Ab probing. **(e)** Disassembly of cilia in MEF cells transfected with control vector or Tctex-1-sh plasmid. The fractions of transfected cells containing a cilium harvested at various time points after serum addition are shown (mean ± s.e.m.; n=3 experiments). **(f)** Immunoblotting assays demonstrated the highly efficient and roughly equivalent uptake of various 9R-peptides. Tctex-1-9R migrated slightly slower than did endogenous (endo) Tctex-1 due to the positive charges of the arginine residues. Mock treated cells were used as controls. **(g)** Immunolabeling of Tctex-1 or GFP for cells transduced with various peptides.

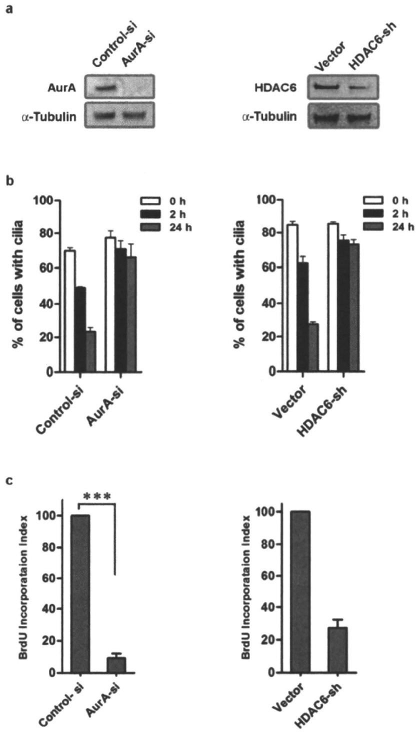

Figure S3 Immunoblotting **(a)**, cilium disassembly (**b**), and BrdU incorporation (**c**) assays of RPE-1 cells transfected with either AurA-si or HDAC6-sh versus controls. All data shown were means ± s.e.m. (n=3 experiments; ***p<0.001, *t*-test).

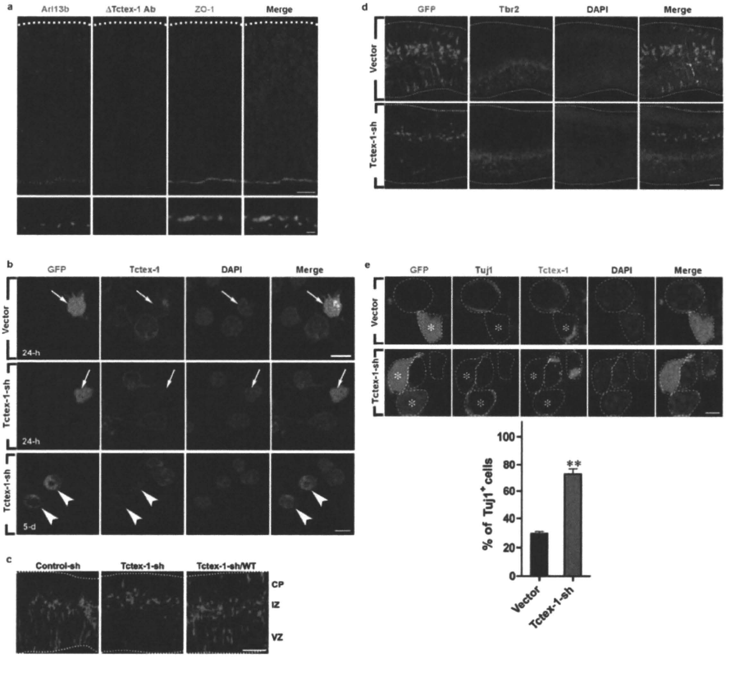

Figure S4 (a) Negative control for the confocal image shown in Fig. 4b by omitting (D) the primary Ab against Tctex-1. Bars= 20 mm (top panel); 2 mm (bottom panel). (**b**) Tctex-1 immunolabeling of cells dissociated from brains electroporated with control vector or Tctex-1-sh 24 hr or 5 days after electroporation. Arrows and arrowheads point to the transfected GFP+ cells harvested at 24-hr and 5-day time points, respectively. (**c**) Brain slices transfected with control-sh, Tctex-1-sh, and Tctex-1-sh/WT plasmids. (**d**) Tbr2 labeling of cortical slices transfected with GFP or Tctex-1-sh plasmid. (**e**) Cells dissociated from brains harvested 40 hr after electroporation were acutely fixed and immunolabeled for Tuj1. Asterisks mark transfected GFP+ cells; dotted lines mark the cell borders. Control transfected cells had a normal level of Tctex-1, and they are often negative for Tuj1. The quantification results show the percentage of GFP+ cells that were also Tuj1 (means ± s.e.m.; n=3 experiments; total of 350 GFP+ cells were scored; **p<0.01 (*t*-test). Bars= 10 mm (a-b, d); 50 mm (c).

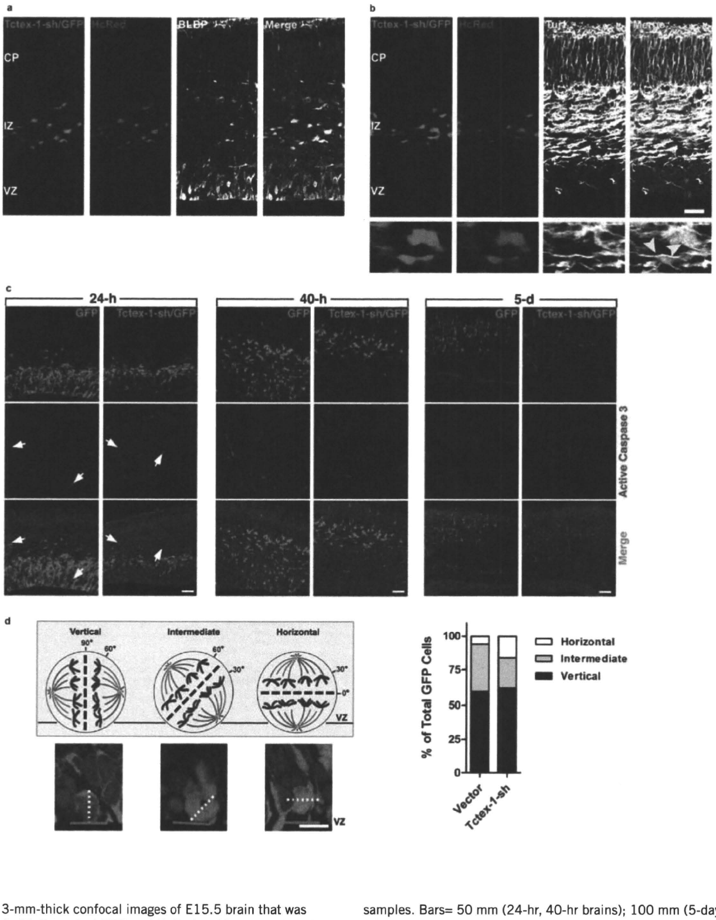

Figure S5 (a, b) 3-mm-thick confocal images of E15.5 brain that was co-electroporated with Tctex-1-sh/GFP and HcRed and immunolabeled for BLBP (a) or Tuj1 (b). Almost all transfected cells were double-positive for both GFP and HcRed. Very few transfected cells were positive for BLBP, whereas a large majority of them exhibited Tuj1. (**c**) Cortical slices, harvested from brain 24 hr, 40 hr or 5 days after electroporation, were labeled for active caspase 3. Arrows pointed to the apoptotic nuclei. Non-specific labeling of blood vessels was also seen in the 40-hr and 5-day samples. Bars= 50 mm (24-hr, 40-hr brains); 100 mm (5-day brain). (d) Schematic drawings (top, left) and representative images (bottom, left) of three alternative orientations of cleavage planes in relation to the ventricular surfaces. Bar=20mm. Based on the alignment of chromosome, the fractions of GFP-labeled dividing cells displayed the vertical cleavage plane (60°-90°), intermediate (30°-60°), and horizontal (0°-30°) were quantified (n=67, 7 brains for GFP transfection, and n=37, 9 brains for Tctex-1-sh/GFP transfection) (right).

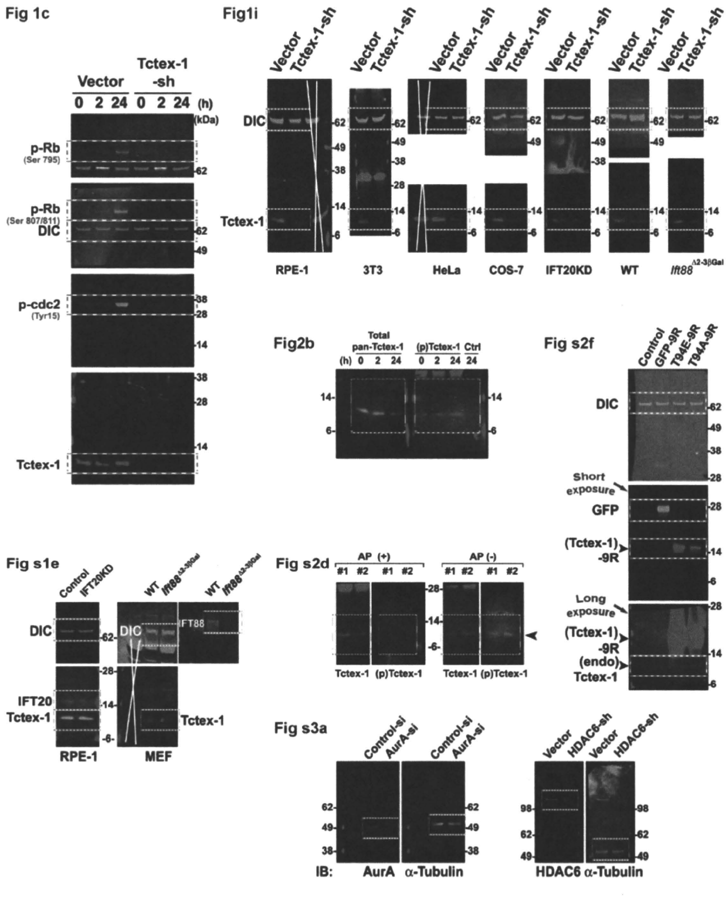

Figure S6 Full scans of Western blots.

THE JOURNAL OF BIOLOGICAL CHEMISTRY VOL. 285, NO. 37, pp. 28425–28433, September 10, 2010

Identification of Eukaryotic and Prokaryotic Methylthiotransferase for Biosynthesis of 2-Methylthio-N^6-threonylcarbamoyladenosine in tRNA

Received for publication, January 22, 2010, and in revised form, June 4, 2010 Published, JBC Papers in Press, June 28, 2010, DOI 10.1074/jbc.M110.106831

Simon Arragain[‡1], Samuel K. Handelman[§¶], Farhad Forouhar[§¶], Fan-Yan Wei[‖2], Kazuhito Tomizawa[‖], John F. Hunt[§¶], Thierry Douki[**], Marc Fontecave[‡ ‡‡], Etienne Mulliez[‡], and Mohamed Atta[‡3]

From the [‡]Institut de Recherches en Technologie et Sciences pour le Vivant IRTSV-LCBM, UMR 5249 CEA/CNRS/UJF, Commissariat à l'Energie Atomique-Grenoble, 17 Avenue des Martyrs, 38054 Grenoble Cedex 09, France, the [§]Northeast Structural Genomics Consortium and [¶]Department of Biological Sciences, Columbia University, New York, New York 10027, the [‖]Department of Molecular Physiology, Faculty of Life Sciences, Kumamoto University, Honjo 1-1-1, Kumamoto 860-8556, Japan, the [**]DSM/INaC/SCIB UMR-E3 CEA-UJF/Laboratoire "Lésions des Acides Nucléiques," Commissariat à l'Energie Atomique-Grenoble, 17 Avenue des Martyrs, 38054 Grenoble Cedex 09, France, and the [‡‡]Collège de France, 11 Place Marcellin-Berthelot, 75005 Paris, France

Bacterial and eukaryotic transfer RNAs have been shown to contain hypermodified adenosine, 2-methylthio-N^6-threonylcarbamoyladenosine, at position 37 (A^{37}) adjacent to the 3′-end of the anticodon, which is essential for efficient and highly accurate protein translation by the ribosome. Using a combination of bioinformatic sequence analysis and *in vivo* assay coupled to HPLC/MS technique, we have identified, from distinct sequence signatures, two methylthiotransferase (MTTase) subfamilies, designated as MtaB in bacterial cells and e-MtaB in eukaryotic and archaeal cells. Both subfamilies are responsible for the transformation of N^6-threonylcarbamoyladenosine into 2-methylthio-N^6-threonylcarbamoyladenosine. Recently, a variant within the human *CDKAL1* gene belonging to the e-MtaB subfamily was shown to predispose for type 2 diabetes. CDKAL1 is thus the first eukaryotic MTTase identified so far. Using purified preparations of *Bacillus subtilis* MtaB (YqeV), a CDKAL1 bacterial homolog, we demonstrate that YqeV/CDKAL1 enzymes, as the previously studied MTTases MiaB and RimO, contain two [4Fe-4S] clusters. This work lays the foundation for elucidating the function of CDKAL1.

The methylthiotransferase (MTTase)[4] family, a subclass of the large radical AdoMet enzyme superfamily, has recently received special attention (1). Indeed, its members catalyze chemically challenging reactions, in all cases involving C–H to C–SCH_3 bond conversion, through a radical mechanism that remains incompletely established. Furthermore, these reactions participate in important biological processes such as tRNA or ribosomal protein modification (2–5). Prototypes for the MTTase family are two bacterial enzymes as follows: MiaB, which modifies N^6-isopentenyladenosine (i^6A) to its 2-methylthio derivative (ms^2i^6A) in tRNA, and RimO, which acts on a specific aspartate residue of the ribosomal S12 protein. Both enzymes have been shown to contain two [4Fe-4S] clusters (4–6). The first one is chelated by the three cysteines of a conserved *CXXXCXXC* motif that is the hallmark signature of the radical AdoMet family (Scheme 1) (7). This cluster serves to bind and reduce AdoMet into methionine and the highly reactive 5′-deoxyadenosyl radical (Ado$^\bullet$) (8). The latter is supposed to abstract an H atom of the substrate (tRNA or protein) selectively, thus generating an intermediate substrate radical that is amenable to C–S bond formation (9). It is believed that the thiolation step involves the second [4Fe-4S] cluster, chelated by three other conserved cysteines in the typical N-terminal UPF0004 domain (Scheme 1) (4–6). The final methylation step involves a second molecule of AdoMet (4–6). A specific signature of the methylthiotransferase subfamily not shared by the other radical AdoMet proteins is the presence of a C-terminal TRAM domain involved in substrate (tRNA or protein) recognition (Scheme 1) (5, 10).

The hypermodified 2-methylthio-N^6-threonylcarbamoyladenosine (ms^2t^6A, where ms stands for methylthio, t for threonine, and A for adenosine) is an anticodon loop modification found at position 37 of tRNAs decoding ANN codons (Scheme 2). Despite the availability of extensive data on the physiological function of this hypermodified base (11–13), its biosynthesis pathway has only been partially characterized. The prerequisite carbamoylation of threonine is an ATP-dependent process requiring threonine and carbonate, but the genes involved in this pathway have remained uncharacterized (14). A recent publication (15) demonstrates that proteins from the YrdC/Sua5 family catalyze the first step in ms^2t^6A biosynthesis, *i.e.* the addition of a threonylcarbamoyl group at the N^6 nitrogen of adenosine converting adenosine 37 to t^6A-37. The second step in ms^2t^6A-37 biosynthesis, including both sulfur insertion and methylation at position 2 of t^6A-37 to yield ms^2t^6A-37, is likely to be catalyzed by one or more MTTases, potentially from the radical AdoMet family.

Bioinformatics analyses presented here demonstrate that five major families of homologous MTTases are encoded in

The nucleotide sequence(s) reported in this paper has been submitted to the GenBank™/EBI Data Bank with accession number(s) BSU25430.

[1] Supported by Région Rhône Alpes CIBLE2010.

[2] To whom correspondence may be addressed. E-mail: fywei@kumamoto-u.ac.jp.

[3] To whom correspondence may be addressed. E-mail: mohamed.atta@cea.fr.

[4] The abbreviations used are: MTTase, methylthiotransferase; t^6A, N^6-threonylcarbamoyladenosine; ms^2t^6A, 2-methylthio-N^6-threonylcarbamoyladenosine; AdoMet, *S*-adenosylmethionine; ms^2i^6A, 2-methylthio-N^6-isopentenyladenosine; ms^2hn^6A, 2-methylthio-N^6-hydroxynorvalyl-carbamoyladenosine.

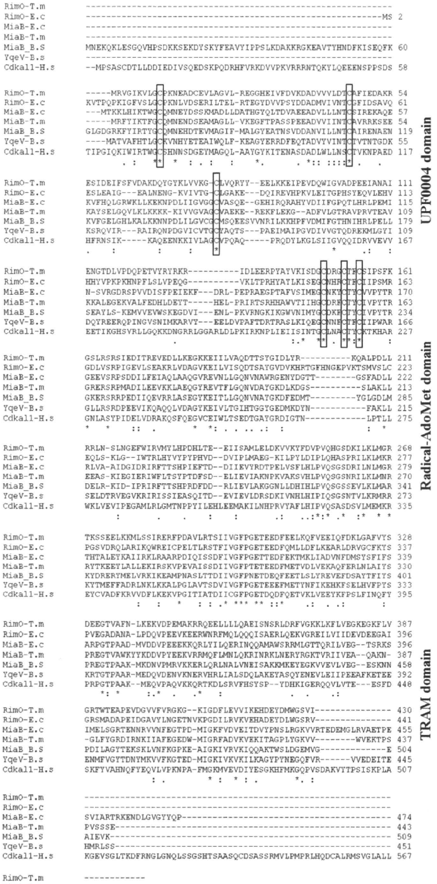

SCHEME 1. **Amino acid sequence alignments of MiaB, RimO, and MtaB (YqeV and Cdkal-1) MTTases from *T. maritima* (*T.m.*), *E. coli* (*E.c.*), *B. subtilis* (*B.sm.*), and *Homo sapiens* (*H.s.*).** The alignment was performed with ClustalW at the EBI site. Totally conserved residues are indicated by asterisks, and conserved cysteine residues are shown in *boxes*. The three domains UPF0004, radical AdoMet, and TRAM are shown on the *right*.

vertebrate and bacterial cells. In addition to the previously characterized MiaB and RimO families, we identify three new families as follows: (i) MtaB found in eubacteria with the *B. subtilis yqeV* gene as its prototype; (ii) e-MtaB found in higher eukaryotes and archaebacteria with the murine *CDKAL1* gene as its prototype; and (iii) MTL1 found so far exclusively in ϵ proteobacteria. *CDKAL1* is of special interest because genetic polymorphisms in this gene increase the reduction of insulin secretion and increase the risk of developing type 2 diabetes (16). Using *in vivo* gene complementation, we show that proteins from both the MtaB and e-MtaB families are responsible for the conversion of N^6-threonylcarbamoyladenosine (t^6A) into 2-methylthio-N^6-threonylcarbamoyladenosine (ms^2t^6A) in tRNA. In addition, using purified preparations of *Bacillus subtilis* YqeV as a representative of the MtaB family, we demonstrate that these enzymes contain two [4Fe-4S] clusters, like the MiaB and RimO families, the only other proven radical sulfur-inserting enzymes.

MATERIALS AND METHODS

Plasmids, Strains, and Growth Conditions—The *Escherichia coli*, *B. subtilis* strains and plasmids used in this study are listed in Table 1. Bacteria were routinely grown in LB medium at 37 °C.

Phylogenomic Analyses—PSI-BLAST profiles (17) created via ClustalW alignment (18) of a set of MiaB and RimO homologs were used to search the human genome and the CRSH data base of proteins of likely equivalent function from 474 bacterial genomes.[5] Sequences identified in this search exhibiting significant (e-value <0.05) sequence similarity to MiaB/RimO that aligned over all three domains were combined with the initial sequences to perform another PSI-BLAST search using the same significance threshold. This second search identified many proteins from other radical AdoMet enzyme families not containing the UPF0004 or TRAM domain, suggesting that all MTTases were likely to have been identified. Cladograms were reconstructed by the program MEGA 3.0 (19) based on 100 bootstrap replicates using the Unweighted Pair Group Method with Arithmetic mean with default parameters. Proteins were assigned to putative functional families via examination of the phylogenetic tree.

Cloning of the yqeV and CDKAL1 Genes and Construction of Overexpressing Plasmids—The open reading frame encoding the YqeV (MtaB1) protein (BSU25430) was PCR-amplified using *B. subtilis* genomic DNA, *Pwo* polymerase (Roche Applied Science), and the following primers: the N-terminal primer (YqeVN-ter, 5′-GAGGTGATCACATATGGCAACTGTTGCTTTC-3′) was designed to contain a unique NdeI restriction site at the predicted initiation codon and the C-terminal primer (YqeVC-ter, 5′-GTGACAGCTCTTTTATTTCTGCAGCTTACAAAC-3′) to hybridize in the 3′-untranslated region and to contain a unique PstI restriction site. The PCR fragment was purified with the High Pure PCR kit (Roche Applied Science), double-digested with NdeI and PstI (Fermentas), and gel-purified before direct cloning into the pT7-7 expression vector, leading to the *pT7-mtab* plasmid. DH5α cells were transformed with the *pT7-mtab* plasmid, and one clone containing an insert with the expected size was selected for sequencing. The cloned *yqeV* was confirmed to be wild type when compared with the GenBank™ accession number BSU25430. Full-length mouse *CDKAL1* cDNA (BC016073) was purchased from Invitrogen. The open reading frame of the

[5] S. K. Handelman and J. F. Hunt, submitted for publication.

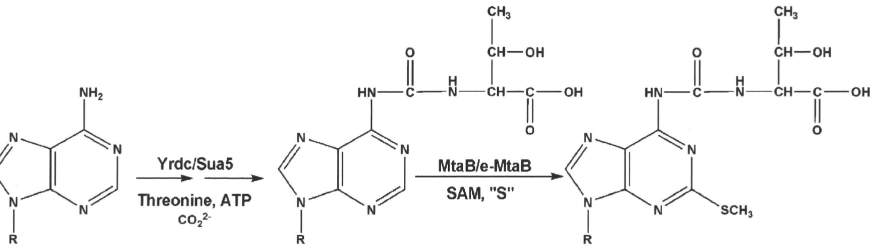

tRNA-A_{37} tRNA-t^6A_{37} tRNA-$ms^2t^6A_{37}$

SCHEME 2. **Biosynthetic pathway for ms^2t^6A.**

TABLE 1

	Genotype	Source
E. coli **strains**		
DH5a	F^-*gyrA96(Nal^r)recA1relA endA1thi-1HsdR17($r_k^-m_k^+$)glnV44 DeoRΔ(lacZYA-argF)U169[Φ80dΔ(lacZ)M15]*	Fermentas
BL21(DE3)	F^-*ompT hsdSB(rB^-,mB^-) gal dcm* (DE3)	Invitrogen
TX3346	F^-*lac1378lacZ-GCGproB$^+$/araΔ(lac-pro)$_{xm}$miaB::Tn10dCm*	29
B. subtilis **strains**		
MGNA-001	*TrpC2*	NIG, Japan
MGNA-C496	*Yqev−*	NIG, Japan
Plasmids		
pT7-7	*ColE1 origin bla, T7 promoter*	30
pGEX6P-1	*Bla*	GE Healthcare
TOPO	*Bla*	Invitrogen
pDB148-Stu	*LacI Pspac ble bla kan*	20

CDKAL1 gene was PCR-amplified to contain SmaI and XhoI restriction sites at the N and C termini, respectively. The PCR fragment was cloned into pCR2.1-TOPO by TOPO-TA cloning (Invitrogen). *CDKAL1* fragment was excised from pCR2.1-TOPO vector by double digestion with SmaI and XhoI (New England Biolabs) and cloned into pGEX6P-1 (GE Healthcare) leading to the *pGEX6P-emtab* plasmid.

yqeV Cloning in pDG148-Stu Plasmid—The following primers were used to amplify *yqeV* gene using *pT7-mtab* as template: pDG148yqeVN, 5′-AAGGAGGAAGCAGGTATGGCAACTGTTGCTTTCCATACGCTTGGCTG-3′ (forward), and pDG148yqeVC, 5′-GACACGCACGAGGTTTAAGAAGACAAACGCATGTGTTCAGTTATTTC-3′ (reverse). The cloning procedure used is exactly as described previously (20). The obtained plasmid was named *pDG148-mtab* and sequenced to verify that no error has been introduced during the PCR experiment. The electrocompetent MGNA-C496 cells were prepared as described and transformed with *pDG148-mtab* by electroporation (21).

Site-directed Mutagenesis; Construction of the AXXXAXXA Triple Variant of the Radical AdoMet Motif—Triple variants of cysteine residues of the *CXXXCXXC* motif were constructed by PCR using the following primers: yqeVCtoA1, 5′-ATACAGGAGGGCGCCAATAATTTCGCCACATTCGCTATCATTCCGTGGGC-3′, hybridized to the noncoding strand, and yqeVCtoA2, 5′-GCCCACGGAATGATAGCGAATGTGGCGAAATTATTGGCGCCCTCCTGTAT-3′, hybridized to the coding strand; Cdkal1CtoA1, 5′-CCATCAACACGGGGGCTCTCAATGCTGCTACCTACGCCAAAACTAAACAC-3′, hybridized to the noncoding strand, and Cdkal1CtoA2, 5′-GTGTTTAGTTTTGGCGTAGGTAGCAGCATTGAGAGCCCCCGTGTTGATGG-3′, hybridized to the coding strand. Mutagenesis was carried out on plasmid *pT7-mtaB* and *pGEX6P-emtab* with QuikChange™ site-directed mutagenesis kits from Stratagene according to the manufacturer's protocol as described previously (22). Mutations were confirmed by DNA sequencing.

Preparation and Analysis of tRNA from B. subtilis—MGNA-001 (wild type) and MGNA-C496 (*yqeV*$^-$) strains were grown in LB medium at 37 °C until the A_{600} reached 1.0. The cells were harvested, and cell-free extract was obtained as described previously (23). Bulk tRNAs were isolated as described previously (24), and 100–200 μg of purified tRNAs were digested to nucleosides by nuclease P1 and bacterial alkaline phosphatase treatment. The resulting hydrolysate was analyzed by HPLC as described previously (24). For the complementation experiment, MGNA-C496 strain lacking the *yqeV* gene was transformed with the expressing plasmid pDG148-*yqeV* coding MtaB protein and grown in LB medium as described previously (20).

Overexpression and Purification of YqeV (MtaB) Protein—The *pT_7-mtab* plasmid was used to transform *E. coli* BL21CodonPlus(DE3)-RIL™, which was grown at 37 °C in Luria Broth supplemented with 100 mg/liter ampicillin. When the A_{600} reached 0.6, the production of the MtaB was induced by addition of 100 μM isopropyl 1-thio-β-D-galactopyranoside, and the incubation was continued for 2 h at 30 °C. The MtaB protein was purified aerobically at 4 °C as follows. The frozen cells were thawed, broken by sonication, and centrifuged at 220,000 × *g* at 4 °C for 1 h. The proteins of the cell-free extract were precipitated with ammonium sulfate between 25 and 55% saturation and dialyzed two times against 60 volumes of 10 mM Tris-HCl, pH 7.5, containing 100 mM KCl (buffer A). The colored solution was then loaded on top of a 30-ml Blue-Sepharose column equilibrated with buffer A. The column was washed with 5 column volumes of buffer A and then eluted with a linear gradient of KCl (0.1–1 M) in buffer A. Fractions containing the MtaB protein were pooled, brought to 1 M ammonium sulfate in Tris buffer, and loaded to a 25-ml butyl-Sepharose FF (GE Healthcare) equilibrated in that buffer. The column was washed with 3 column volumes of buffer A, and the pure protein was eluted with a descending gradient (1–0 M) of ammonium sulfate buffer A. The fractions containing MtaB were pooled, concentrated by ultrafiltration using an Amicon cell fitted with a YM30 (Diaflo), and submitted to a final purification on an analytical Superdex-75 gel filtration column using Tris-HCl, pH 8.0, containing 0.25 M KCl and 5 mM DTT. The fractions were analyzed by SDS-PAGE (12%), and the most pure were pooled, concentrated, and stored at 77 K.

Preparation of the Apoprotein—The apo-form of MtaB protein was prepared as described previously (6).

Reconstitution of ApoMtaB—Fe-S cluster reconstitution into *B. subtilis* MtaB was carried out under strictly anaerobic conditions into a Jacomex NT glovebox containing less than 2 ppm O_2 as described previously (6).

Analytical Methods—Quantitative amino acid analysis was used to determine extinction coefficients of purified *B. subtilis* MtaB: $\epsilon_{280} = 46.8$ mM^{-1}cm^{-1} for the apoenzyme; $\epsilon_{280} = 87.8$ mM^{-1}cm^{-1} and $\epsilon_{400} = 30.0$ mM^{-1}cm^{-1} for the holo-enzyme (*i.e.* an A_{400}/A_{280} ratio of 0.34). Iron and inorganic sulfide were quantified as described previously (25). tRNAs were digested and analyzed by HPLC as described previously (24).

Mass Spectrometry Analysis—HPLC-tandem mass spectrometry analyses were performed with a 1100 Agilent chromatographic system coupled with an API 3000 triple quadrupolar apparatus (PerkinElmer Life Sciences) using a turbo ion spray electrospray source in the positive mode. HPLC separation was carried out on a 2 × 150-mm column containing 3 μm of octadecylsilyl silica gel (Uptisphere, Interchim Montluçon, France) using a gradient of acetonitrile in 5 mM ammonium formate. Acetonitrile content was increased from 0 to 40% over the first 20 min and then held constant for 40 min. The settings of the tandem mass spectrometer were optimized by injection of a pure solution of i^{6}A to favor loss of the ribose unit upon collision-induced fragmentation. Mass spectrometry detection was carried out in neutral loss mode to obtain a high specificity. In this configuration, pseudo-molecular ions ($[M + H]^+$) and fragments ($[M - 132 + H]^+$) obtained by collision in the second quadrupole (collision) cell were analyzed in the first and third quadrupoles, respectively. Using this approach, only nucleosides losing their ribose unit were detected. The pseudo-molecular ion of the latter compounds was monitored in a 300–450 mass range.

Light Absorption Spectroscopy—UV-visible absorption spectra were recorded under anaerobic conditions in a glove box on an XL-100 Uvikon spectrophotometer equipped with optical fibers.

EPR—X-band EPR spectra were recorded on a Bruker ESP-300E EPR spectrometer operating with an ER-4116 dual-mode cavity and an Oxford Instrument ESR-9 flow cryostat.

RESULTS AND DISCUSSION

Phylogenomic Analysis of Radical AdoMet Methylthiotransferases—Sequence profiling techniques were used to search 474 bacterial genomes and the human genome for families of radical AdoMet MTTase. To ensure full coverage of this enzyme class, iterative expansion of the sequence profile was continued until radical AdoMet enzymes with different overall domain architecture were identified by the profile (see under "Materials and Methods"). Five distinct sequence families with representatives in at least three genomes were identified in this manner (Fig. 1). Proteins in all of these families have an N-terminal UPF0004 domain with three invariant cysteines in the $CX_{34-36}CX_{28-37}C$ motif, a central radical AdoMet domain with three invariant cysteines in CX_3CX_2C motif, and a C-terminal TRAM domain (Scheme 1) (3, 5).

Two of the five MTTase families identified in our analyses represent the well characterized MiaB and RimO enzyme families (4–6). The human and *B. subtilis* genomes both encoded a member of the MiaB family (*CK5RAP1* and *YmcB/BSU17010*, respectively) in addition to a member of another MTTase family. The third MTTase family identified in our analyses includes *yqeV* (BSU25430), the other MTTase encoded in the *B. subtilis* genome, whose enzymatic activity was characterized in this study. We have designated this family MtaB, for methylthio-threonylcarbamoyl-adenosine transferase B, because it performs the second step in the biosynthesis of this hypermodified base (Scheme 2). This nomenclature was chosen for consistency with the name of MiaB, which performs the second step in biosynthesis of methylthio-isopentenyl-adenosine. The fourth MTTase family includes enzymes of unknown substrate specificity that are found exclusively in ϵ proteobacteria, including the pathogens in the *Helicobacter* and *Campylobacter* genera. We have designated this family MTL1, for methylthiotransferase-like family-1. The fifth and final MTTase family includes CDKAL1, the other MTTase encoded in the human genome, whose enzymatic activity is also characterized in this study. We have designated this family e-MtaB for eukaryotic methylthiothreonylcarbamoyl-adenosine B, because it performs probably the second step in the biosynthetic pathway (Scheme 2). The e-MtaB family is not found in any eubacteria genome in our data base, but it is found in a variety of archaebacteria, as opposed to the other four MTTase families. Notably, this family is not represented in any eubacterial genome. All five families are approximately equally remote from one another, suggesting that functional differences between these families were established at an early evolutionary time.

Combining these phylogenomic results with the previously established occurrence of hypermodified adenosines ms^{2}i^{6}A and ms^{2}t^{6}A in both *B. subtilis* and human tRNAs (26, 27), we hypothesized that both MtaB and e-MtaB enzyme families are likely to catalyze the methylthiolation of t^{6}A to form ms^{2}t^{6}A (Scheme 2). Because previously characterized MiaB family members all catalyze biosynthesis of ms^{2}i^{6}A (22, 28), the MiaB

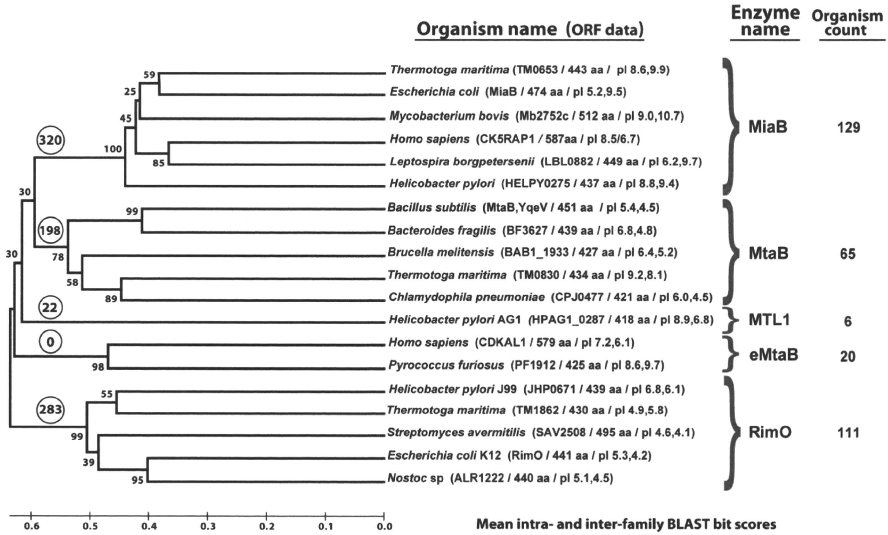

Mean intra- and inter-family BLAST bit scores

	MiaB	MtaB	MTL1	eMtaB	RimO
MiaB	**397**	179	144	157	161
MtaB		**289**	177	134	131
MTL1			**520**	118	112
eMtaB				**279**	122
RimO					**375**

FIGURE 1. **Phylogenomic analysis of bacterial and human radical AdoMet methylthiotransferases.** The cladogram shows the inferred evolutionary distances between representatives of all homologous protein families identified in a systematic search of the human genome and 474 fully sequenced bacterial genomes (see "Materials and Methods"). The MiaB and RimO families have been biochemically characterized in previous literature. This study described initial experimental characterization of representatives from the methylthiothreonylcarbamoyladenosine transferase B (MtaB) family and the eukaryotic methylthiothreonylcarbamoyladenosine transferase B (e-MtaB) family. The methYthiotransferase-like family 1 (MTL1), which is restricted to ϵ proteobacteria, has yet to be characterized experimentally. The e-MtaB family is found in archaebacteria but not eubacteria, although the other four families are found in eubacteria but not archaebacteria. The organism count indicates the number of unrelated bacterial genomes that encode a representative of each family (*i.e.* after correction for redundancy in genome organization). The *numbers in circles* at the root of each family indicate the number of times a member of one of the other families shown here is encoded simultaneously in the same genome (without redundancy correction). The *numbers in a smaller font* near the branch points indicate the percent of MEGA bootstrap replicates with the illustrated relative ordering of the successive branch points. Splits between the identified families confidently precede those within the families, with 100, 78, 98, and 99% confidence. Proper grouping of proteins in the MtaB family, which has the lowest 78% confidence for its first internal split, is supported by PSI-BLAST sequence profiling (data not shown) as well as the fact that proteins assigned to this family are never encoded in the same genome, even though 198 members of the other families are found encoded in the same genome as MtaB family members. The ORF data in *parentheses* includes the name of the protein, its amino acid sequence length, its overall pI, and the pI of its TRAM domain. The TRAM domains of bacterial MiaBs are generally basic, although those of bacterial RimOs are generally acidic. The TRAM domains of members of the other families show wider variations in pI values.

family members encoded in the *B. subtilis* and human genomes are likely to be responsible for the observed biosynthesis of ms^2i^6A. Because only one additional MTTase family is encoded in each of these genomes, the corresponding MtaB and e-MtaB enzymes are leading candidates to catalyze the biosynthesis of ms^2t^6A, the only other methylthiolated base observed in these organisms. We therefore undertook experimental studies to critically evaluate this bioinformatics-based inference.

YqeV/MtaB and CDKAL1/e-MtaB Transform t^6A into ms^2t^6A in Vivo—To test the function of the corresponding proteins, we assayed the influence of the *yqeV* and *CDKAL1* genes on tRNA modification *in vivo* in *E. coli* strain TX3346, which lacks a functional *miaB* gene. This strain has the advantage of accumulating i^6A-37, as a consequence of the inactivation of the *miaB* gene, and also containing t^6A-37, because *E. coli* K12 does not encode any enzyme-catalyzing methylthiolation of this nucleoside. The TX3346 strain was transformed with either plasmid *pT_7-mtab* expressing the *B. subtilis yqeV/mtaB* gene or plasmid *pT7-emtab* expressing the human *CDKAL1/e-MtaB* gene. Bulk tRNAs were isolated after growth at 37 °C, hydrolyzed, and processed for HPLC analysis of their modified nucleosides, as described previously (24). Under these conditions, chromatograms of tRNA hydrolysates from the control TX3346 strain showed, as expected, both t^6A-37 and i^6A-37

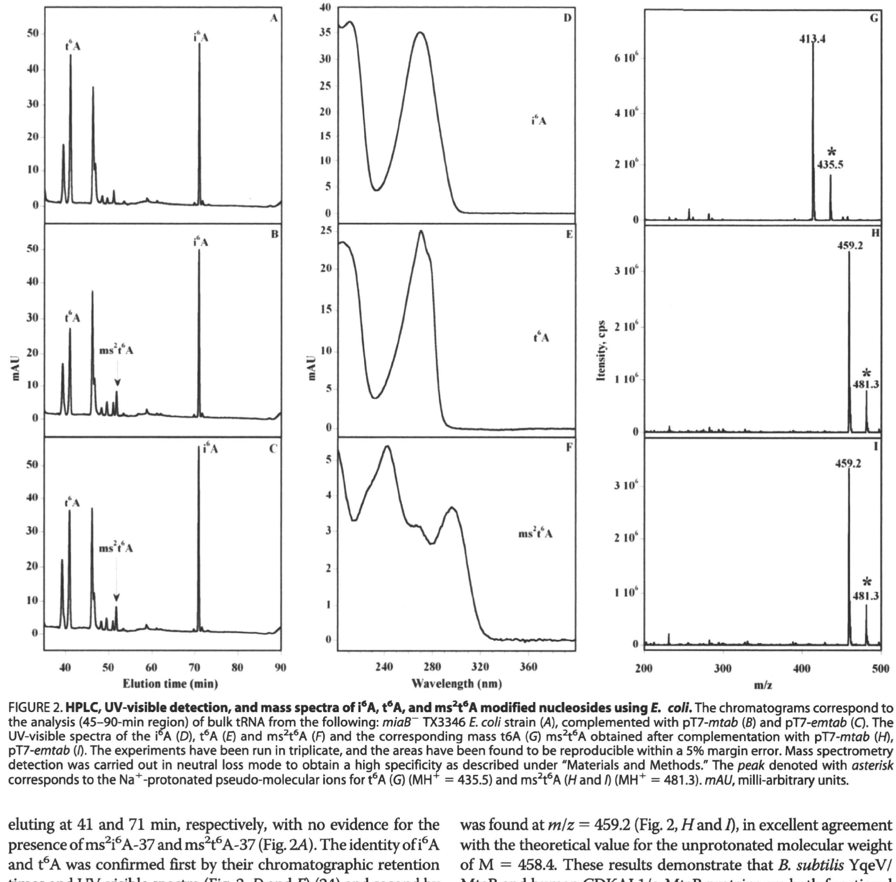

FIGURE 2. **HPLC, UV-visible detection, and mass spectra of i^{6}A, t^{6}A, and ms^{2}t^{6}A modified nucleosides using *E. coli*.** The chromatograms correspond to the analysis (45–90-min region) of bulk tRNA from the following: *miaB*$^-$ TX3346 *E. coli* strain (*A*), complemented with pT7-*mtab* (*B*) and pT7-*emtab* (*C*). The UV-visible spectra of the i^{6}A (*D*), t^{6}A (*E*) and ms^{2}t^{6}A (*F*) and the corresponding mass t6A (*G*) ms^{2}t^{6}A obtained after complementation with pT7-*mtab* (*H*), pT7-*emtab* (*I*). The experiments have been run in triplicate, and the areas have been found to be reproducible within a 5% margin error. Mass spectrometry detection was carried out in neutral loss mode to obtain a high specificity as described under "Materials and Methods." The *peak* denoted with *asterisk* corresponds to the Na$^+$-protonated pseudo-molecular ions for t^{6}A (*G*) (MH$^+$ = 435.5) and ms^{2}t^{6}A (*H* and *I*) (MH$^+$ = 481.3). *mAU*, milli-arbitrary units.

eluting at 41 and 71 min, respectively, with no evidence for the presence of ms^{2}i^{6}A-37 and ms^{2}t^{6}A-37 (Fig. 2*A*). The identity of i^{6}A and t^{6}A was confirmed first by their chromatographic retention times and UV-visible spectra (Fig. 2, *D* and *E*) (24) and second by coupled HPLC/mass spectrometry analysis. The latter revealed the presence of a compound eluting at 41 min that could be assigned to t^{6}A on the basis of the *m/z* ratio of its protonated pseudo-molecular ion (MH$^+$ = 413.4) (Fig. 2*G*), in good agreement with the theoretical value for the unprotonated molecular weight of M = 412.4. In contrast, HPLC analysis of tRNA extracted from the *E. coli* TX3346 transformed with either plasmid *pT$_7$-mtab* or plasmid *pT$_7$-emtab* clearly showed no evidence for the presence of ms^{2}i^{6}A in the chromatogram, with the peak corresponding to i^{6}A remaining essentially unchanged in intensity and the presence of a new peak eluting at 52 min (Fig. 2, *B* and *C*). The elution time (Fig. 2, *B* and *C*) and UV-visible spectrum (Fig. 2*F*) of the new peak are identical to that of ms^{2}t^{6}A (24). By HPLC/MS, the corresponding protonated pseudo-molecular ions MH$^+$ was found at *m/z* = 459.2 (Fig. 2, *H* and *I*), in excellent agreement with the theoretical value for the unprotonated molecular weight of M = 458.4. These results demonstrate that *B. subtilis* YqeV/MtaB and human CDKAL1/e-MtaB proteins are both functional *in vivo* and selectively involved in the conversion of t^{6}A to ms^{2}t^{6}A.

Whether the predicted iron-sulfur cluster common to all members of the radical AdoMet family was required for activity was investigated by studying site-directed mutants in which the three conserved cysteines of the conserved CXXXCXXC sequence in MtaB and e-MtaB have been changed to alanine. Using the *in vivo* assay described above, we found that the *miaB*$^-$ *E. coli* TX3346 strain transformed with *pT7-mtaB-Cys-Ala* and *pGEX6P-emtab-Cys-Ala* was unable to produce the ms^{2}t^{6}A-modified nucleoside (data not shown). This provides, as expected, strong evidence that the cluster is required for activity.

In Vivo Experimental Validation of the Function of YqeV/MtaB by Using B. subtilis MGNA-C496 Strain—To obtain further evidence that MtaB from *B. subtilis* is the enzyme that is